J Mater Sci (2007) 42:2618–2629
DOI 10.1007/s10853-006-1342-7

Positron lifetime studies and coincidence Doppler broadening spectroscopy of Al–6Mg–*x*Sc (*x* = 0 to 0.6 wt.%) alloy

M. S. Kaiser · P. M. G. Nambissan · M. K. Banerjee · A. Sachdeva · P. K. Pujari

Received: 7 May 2005 / Accepted: 6 March 2006 / Published online: 4 January 2007

Abstract Positron annihilation spectroscopy (PAS), comprising of both positron lifetime and coincidence Doppler broadening measurements, has been employed for studying the phase decomposition behaviour of scandium doped Al–6Mg alloys. Micro structural and age hardening studies have also been conducted to substantiate the explanation of the results of PAS. Samples with scandium concentration ranging from 0 to 0.6 wt.% have been studied. The measured positron lifetimes of undoped alloy reveal that GP zones are absent in the as-prepared Al–6Mg alloy. The observed positron lifetimes and the results of coincidence Doppler broadening measurements largely stem from the entrap of positrons at the interface between aluminium rich primary dendrites and the magnesium enriched interdendritic eutectic mixture of Mg_5Al_8 (β) and the primary solid solution of aluminium (α). The study also provides evidence of the formation of scandium vacancy complexes in Al–6Mg alloys doped with scandium upto a concentration of 0.2 wt.%. However such complex formation ceases to continue beyond 0.2 wt.% Sc; instead, the formation of fine coherent precipitates of Al_3Sc is recorded in the as prepared alloy containing 0.6 wt.% scandium. The positron annihilation studies coupled with CDBS have also corroborated with the fact that the fine coherent precipitates of Al_3Sc are formed upon annealing the Al–6Mg alloys doped with scandium of concentration 0.2 wt.% and above. Transmission electron microscopic studies have provided good evidence of precipitate formation in annealed Al–6Mg–Sc alloys. Elevated temperature annealing leads to dissociation of the scandium-vacancy complexes, thereby leading to the enhancement of the mobility of magnesium atoms. This has facilitated fresh nucleation and growth of Mg_5Al_8 precipitates in the above alloys at 673 K.

M. S. Kaiser
Bengal Engineering and Science University,
Howrah 711103, West Bengal, India

P. M. G. Nambissan (✉)
Saha Institute of Nuclear Physics, 1/AF Bidhannagar,
Kolkata 700064, India
e-mail: pmg.nambissan@saha.ac.in

M. K. Banerjee
Government College of Engineering and Ceramic
Technology, 73 A.C.B. Lane, Kolkata 700010, India

A. Sachdeva · P. K. Pujari
Radiochemistry Division, Bhabha Atomic Research Centre,
Mumbai 400085, India

Introduction

Al–Mg alloys are known to be commercially attractive for structural applications including ship structures, due to its excellent resistance to sea water corrosion, greater weldability, higher ductility and adequate strength [1, 2]. Similar to many other aluminium alloys, Al–Mg alloy system exhibits a decreasing solid solubility of magnesium with decreasing temperature. However, in spite of the existence of a sloping solvus in the phase diagram of the Al–Mg alloy system, no significant strengthening is experienced in the concerned alloy through precipitation hardening mechanism [3]. Reportedly the decomposition of supersaturated Al–Mg alloy takes place by the

formation of globular Mg_5Al_8 at grain boundaries as the divorced eutectic when the solidified alloy is annealed out at elevated temperature [4]. A number of earlier workers propounded that the binary Al–Mg alloy did not behave like the common age hardenable aluminium alloys, which are known to form GP zones and intermediate precipitates during the course of ageing from the solutionised and quenched state. These zones or intermediate precipitates are mostly coherent or semicoherent with the matrix. As a result of interaction between the moving dislocations and the coherency strain fields existing around them, the alloys are found to be age hardened quite significantly. On the contrary, binary Al–6Mg alloy cannot be hardened by such mechanism since its GP solvus is stated to lie below room temperature [5]. The role of quenched-in vacancies in the formation of small spherical GP zones in Al–Mg alloys and the subsequent precipitation of the β-phase (Mg_5Al_8) are also documented in literature [6, 7]. In order to achieve a strength value comparable to other precipitation hardenable aluminium alloys, an attempt to make use of a higher amount of Mg (~10 wt.%) has resulted in greater processing challenges with high proneness to stress corrosion cracking [8, 9].

Trace additions are known to modify the structure and properties of a large number of aluminium alloys in various ways [10]. To make Al–Mg alloy competitive with other low density systems for high performance applications, scandium has been added as a potent hardener [11, 12]. Scandium as a minor additive to Al–Mg alloy combines with aluminium to form coherent Al_3Sc phase of LI_2 structure [13] and appreciably strengthens the alloy through precipitation hardening [14, 15]. Scandium when added by 0.2 wt.% is known to form complexes with quenched-in vacancies in Al–Mg (Sc) alloy. These complexes aid in nucleation of precipitates and hence consequent hardening [16]. In fact many effects of trace additions are linked with their interaction with vacancies.

Positron annihilation spectroscopic techniques help in monitoring the interaction of the solute atoms with the vacancies by virtue of the sensitivity of positrons to vacancy type sites for getting trapped and annihilated [17, 18]. In view of the fact that precipitation phenomenon in an alloy system is largely influenced by the crystal defects, there has been considerable interest in using positron annihilation spectroscopic methods for studying the phase decomposition phenomenon in different alloy systems [17]. Positrons may be entrapped at the zones and precipitates formed during the decomposition of supersaturated solid solutions. Hence the annihilation parameters of positrons directly reflect the type of positron localization and the chemical composition of the sites, which trap and annihilate positrons. Although phase decomposition behaviour of a large number of Al–Mg alloys is reported to have been studied with the help of this technique [19], there has been no report as yet on the use of positron annihilation method for understanding the phase transformation effected in Al–Mg alloy doped with scandium. Keeping in view of the worth of scandium as a trace additive to Al–Mg alloy, the present paper has dealt with the application of positron annihilation method for understanding the exact mechanism through which scandium precipitates in Al–6Mg alloy. Other supportive experimental results are also used to substantiate our findings on the role of scandium as a potential trace additive to Al–6Mg alloy in securing appreciable precipitation hardening.

Experimental

Following the procedure reported elsewhere [20], melting was carried out in a resistance-heating pot furnace under the suitable flux cover. Several cycles of solidification and melting were done to achieve uniform composition of binary Al–Mg and ternary Al–Mg–Sc alloys of varying Sc content. Commercially pure aluminium (99.5% purity) was taken as the starting material. At first, elemental aluminium and the aluminium–scandium master alloy (2%Sc) were melted in a clay-graphite crucible. Magnesium ribbon (99.7% purity) of requisite quantity was then added into the melt. The molten alloys were solidified in a metal mould. The alloys solidified at 20 K s^{-1} were then cut into suitable pieces for subsequent characterization.

Positron lifetimes were performed by using a 400 kBq strong ^{22}Na source sandwiched between two specimens ($10 \times 10 \times 2$ mm) of the sample and by recording the spectra using a slow-fast coincidence set-up employing BaF_2 scintillators and XP2020Q photomultiplier tubes. The time resolution of the spectrometer was about 200 ps (fwhm) for the coincidence spectrum of the gamma rays from ^{60}Co source. About 1.5×10^6 counts were collected under each spectrum to have a good peak to background ratio (>5000:1) and the spectra were analysed using RESOLUTION and POSITRONFIT [21].

Doppler broadening measurements, to enable the estimation of the *S* and *W* parameters, were carried out using an HPGe detector with energy resolution 1.26 keV at 514 keV (^{85}Sr) using 2 μs shaping time in the amplifier. A NaI(Tl) scintillator with photomultiplier tube was used to record the outgoing 511 keV

gamma ray and the coincidence pulse generated from the output signals from the two detectors was used to gate the spectra so as to minimize the background. More than 300,000 counts were collected at the peak and the peak to background ration in this case was above 20,000:1.

The coincidence Doppler broadening spectroscopic (CDBS) experiments were conducted with the help of a 600 kBq strong ^{22}Na source and using two HPGe detectors facing the source-sample sandwich from opposite sides. The energies E_1 and E_2 of both the annihilation gamma rays are measured and a two-parameter spectrum is generated with $E_1 + E_2$ and $E_1 - E_2$ on the two coplanar perpendicular axes. The sum of the two energies represents the total rest mass energy of the electron and positron less the electron binding energy ($2m_0c^2 - E_B$) while the difference directly gives the magnitude of the Doppler shift in terms of the longitudinal component of the electron momentum in the direction of detection of the gamma rays ($\Delta E = p_L c/2$). The coincidence events falling within a selected window $2m_0c^2 - 2.8$ keV $< (E_1 + E_2) < 2m_0c^2 + 2.8$ keV are collected to obtain a nearly-background-free Doppler broadened annihilation gamma ray lineshape with peak to background ratio better than 100,000:1. This enables us to extract precise information about the elemental signatures of positron trapping sites from the high momentum region of the spectra [22]. Further details of data analysis are described afterwards.

Isochronal annealing of two selected samples was performed in a high vacuum ($P < 0.75$ mPa) furnace for 1 h at different temperatures ranging from 373 K to 873 K. Positron annihilation measurements were performed after slowly cooling (~50 K/h) the samples to room temperature. The temperature stability was maintained within ±1 K during each annealing treatment. The good vacuum conditions helped to ensure that the samples were free of any surface contamination or quenching effects after the annealing.

Results and discussion

The as-prepared samples

A knowledge about the microstructural conditions existing within the experimental alloys will be quite helpful in explaining the results of positron annihilation spectroscopy. A limited amount of information only is obtainable from the optical metallographic study. The optical microstructure of the as prepared binary alloy (undoped) is seen comprised of dendrites of α and the black interdendritic constituents (Fig. 1). While α refers to the aluminium rich solid solution, the eutectic mixture consists of a lamellar aggregate of α and Mg_5Al_8 (β). Doping of Al–6Mg alloy by scandium leads to an increase in solidification speed, thereby reducing both the size and the number density of second phase (eutectic) constituents (Fig. 2). Dendrite arm spacing in doped alloys are found to be within a range of 20–40 μm.

When the solidified Al–6Mg–0.2Sc is annealed at a high temperature (~473 K), precipitation of coherent Al_3Sc phase is found to take place (Fig. 3). Deformation contrast as observed in Fig. 3 is the evidence of coherency of the Al_3Sc precipitates. While the precipitate size approximately is around 10 nm, the average interparticle distance is found to be roughly 100 nm.

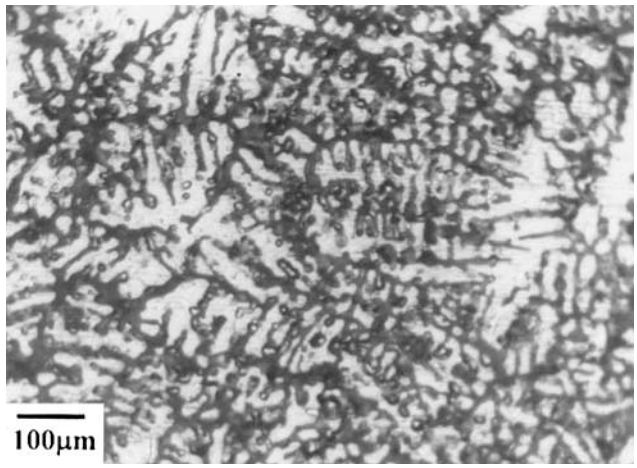

Fig. 1 Optical microstructure of undoped alloy showing dendrites of α and magnesium-rich eutectic (black)

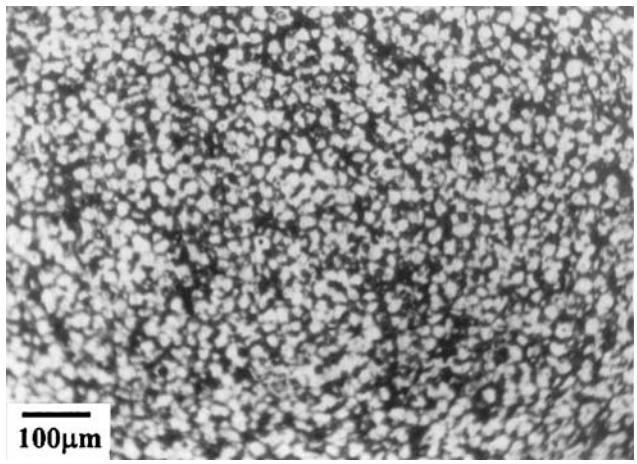

Fig. 2 Optical microstructure of Sc-doped alloy showing refinement of structure

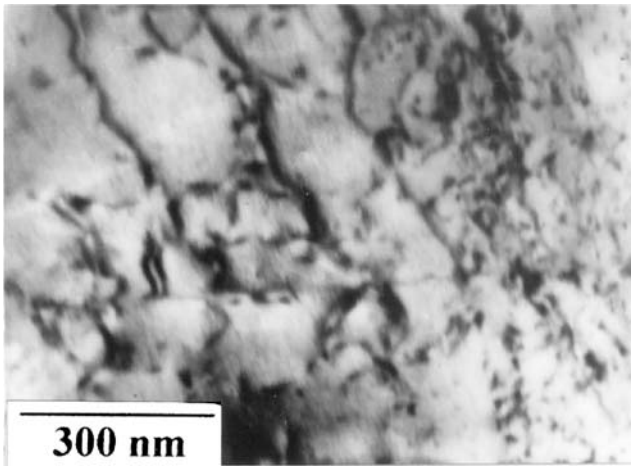

Fig. 3 Transmission electron microscopic image of Al–6Mg–0.2Sc annealed at 473 K

However, alloy with higher scandium content (~0.6 wt% Sc) is found to contain fine Al_3Sc precipitates even in its as prepared state (Fig. 4).

The positron lifetime spectra of all the samples, both in the as-cast state as well as after the isochronal annealing, gave two lifetimes τ_1 and τ_2 with relative intensities I_1 and I_2. To understand about the origin of these two lifetimes, we first consider the case of the scandium-free alloy Al–6Mg in which we obtained $\tau_1 = 120$ ps and $\tau_2 = 249$ ps. The magnitude of the longer lifetime τ_2 is close to the positron lifetime in monovacancies in Mg, which has been reported as 250 ps [23]. But the lifetime in monovacancies in Al is also well known as 253 ps [24]. Within the error bars, therefore, it is difficult to pinpoint about the species of the vacancies. The results of the CDBS measurements

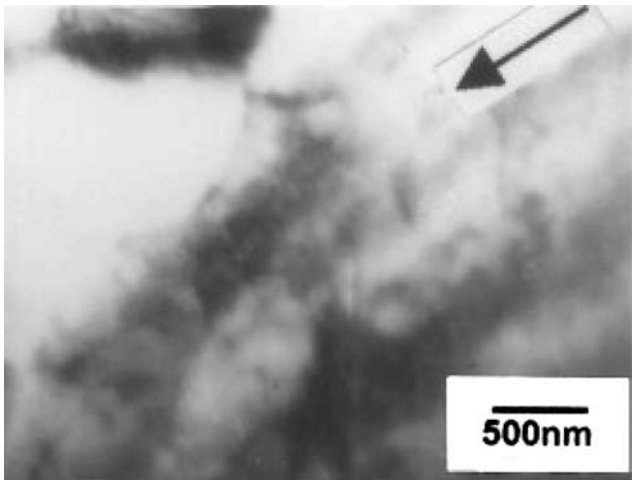

Fig. 4 Transmission electron microscopic image of Al–6Mg–0.6Sc in the as-prepared state

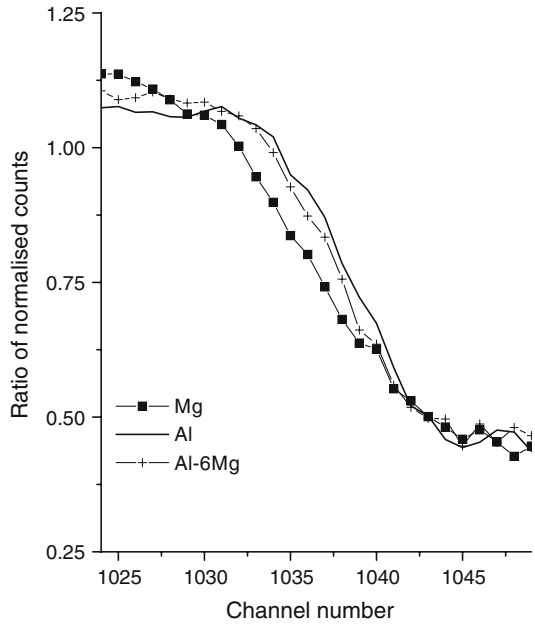

Fig. 5 Coincidence Doppler broadened (CDB) spectra of Al, Mg and Al–6Mg alloy

shown in Fig. 5 may help to some extent to remove this ambiguity. What has been depicted in the figure is the $511 + \Delta E$ part of the gamma ray spectra of the three samples, divided by the corresponding spectrum of a reference silver sample after the normalization of the area under the curves. Within the level of possible uncertainties in the data (the average error bars lie within the size of the points), the curve for Al–6Mg sample is found to lie closer to that of Al than that of Mg. Since these are regions where the events due to the annihilation by core electrons are populated, ΔE which is related to p_L will impart the signature of the element, which the annihilated electrons belonged to. Thus it appears that a given annihilation site or the resultant event is more influenced by the electrons of Al and less by those of Mg. It is to be noted that the curve of Al–6Mg does not overlap fully with either Al or Mg. This observation is suggestive of the fact that the trapping of positrons does not occur in a pure Al environment or in that of Mg. Rather the annihilation sites seem to be some kind of interface between the two constituent elements. It thus appears that there has been local segregation of Mg atoms. It is not out of place to mention that a high density of vacancy loops have been noted in quenched binary Al–Mg alloy. In certain Al-based alloys, positrons have been found trapped in coherent GP zones free of any vacancies [19]. If it were so in our experimental alloy as well, a modified single bulk lifetime characteristic of the element constituting the GP zone should have been

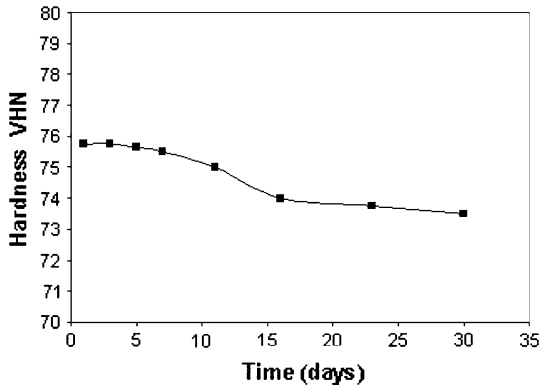

Fig. 6 The natural aging curve of Al–6Mg alloy

obtained as a result of saturation trapping. However, we have seen the effect of trapping as a two-component positron lifetime spectrum. Hence the possibility of the formation of GP zones in the solidified Al–6Mg alloy is reasoned out. This conjecture is supportive of the earlier reports advocating that GP zones could not form in Al–Mg alloys [5]. In GP zones forming age hardenable aluminium alloys, GP zone density increases with increasing natural ageing time of the solutionised and quenched alloy. Increasing number of zones envisages an appreciable hardening of the alloys during natural ageing. However, natural ageing of the present Al–6Mg alloy does not exhibit any increase in hardness (Fig. 6). This observation favours the argument that GP zones do not form in the as prepared Al–6Mg alloy. However, having the signatures of both the elements in the annihilation curve, as shown in Fig. 5, it is prudent to assume that the trapping centers are some kind of interface separating the Mg-rich region from a pure Al-rich region.

The question whether the trapping sites are really vacancies can also be addressed in a different way. The bulk positron lifetime in Al–6Mg, calculated by giving appropriate weights by ratio or atomic percentage as coefficients to the known positron lifetimes in Al (165 ps) and Mg (225 ps), is obtained as 169 ps. Using this value and assuming a two-state trapping model [25] to prevail in the sample, the expected value of the shorter lifetime τ_1 can be calculated as

$$\frac{1}{\tau_1^{\text{cal}}} = \frac{1}{\tau_f} + \kappa \tag{1}$$

where the positron trapping rate κ is given by

$$\kappa = \frac{I_2}{I_1}\left(\frac{1}{\tau_f} - \frac{1}{\tau_2}\right) \tag{2}$$

The estimation yields 137 ps whereas the measured value of 120 ps is lower than this. From Eq. (1), a reduced value of τ_1 will imply an increased concentration of positron trapping sites, as the trapping rate given by Eq. (2) is also related to the trap concentration C through the relation $\kappa = \mu C$. (μ is the specific trapping rate.) Thus it appears that, apart from the inherently in-built monovacancies, other kinds of structural defects are also present in the sample. The formation of an interface between the Mg-rich regions and Al may be a possibility. In this case, positrons are trapped and localized by such interfaces. In the experimental sample, it is to be presumed that the above interface separates the Mg-rich regions from the bulk Al matrix. If we now presume that the aforementioned Mg-rich regions are essentially GP zones, an order of magnitude estimation of such areas may be obtained from the relation

$$r_p = \frac{\kappa}{4\pi D_+ N} \tag{3}$$

Here D_+ is the positron diffusion constant in Mg ($0.5\ \text{cm}^2\ \text{s}^{-1}$) and N is the average number of such particles. If N is taken approximately as 10^{15} per cm^3 [19], the radius of the Mg regions may be obtained as 2.2 nm and is much smaller than the thermal diffusion length (~260 nm) for positrons in Mg [26]. Moreover, it is hardly sensible to appreciate that an incoherent interface is present around a cluster of magnesium atoms (GP zones) of size around 2.2 nm. Therefore, any presumption that the Mg-rich regions in question are actually GP zones would always fail to explain the experimentally observed lifetime of positrons, which are only attributable to the trapping of positrons at grain boundary type incoherent interfaces. It is not out of place to mention that there is report on the formation of spherical GP zones in binary Al–6Mg alloy [6, 7]. However, a number of earlier findings have also recorded that the GP solvus of the experimental alloy system lies below room temperature over a wide range of compositions [5]. Hence it is clear that the experimental alloy samples, cast at room temperature, do not contain GP zones, notwithstanding if spherical zones as reported elsewhere are truly formable in Al–6Mg alloy or not.

Importantly, the optical microstructure of the experimental alloy clearly delineates that the primary dendrites of α (Al-rich region) entrap $\alpha + \beta$ (Mg_5Al_8) eutectic rich in magnesium (Fig. 3). The size of the primary crystallites has been measured to be around 15–20 μm whereas it is evident from the micrographs

that the black Mg rich eutectic is at least one order of magnitude smaller in size. It may be considered that the interfaces separating primary α from the β-rich eutectic are chiefly responsible for positron annihilation. As stated earlier, the black eutectic phase has lamellar structure and hence the incoherent interplanar boundaries within the lamellar structure may also act as positron annihilation sites. However in that case, the chemical environment around the positron trapping sites would have been relatively richer in magnesium concentration. Implicitly, CDBS curve for the concerned alloy would not have then been so close to Al-line as shown in Fig. 5; rather it would have been shifted more towards the CDBS curve for magnesium. Hence it is to be accepted that the majority of positron annihilation has taken place at the eutectic interface.

With the addition of Sc in the matrix, the positron lifetimes (both τ_1 and τ_2) decrease initially till the concentration of the doped Sc reaches 0.2 wt.% and increase with further doping after it. The intensity I_2 shows the opposite behaviour. These changes are illustrated in Fig. 7. The S and W parameters also show a reversal of changes around a Sc concentration of 0.2, as shown in Fig. 8, showing perfect consistency of variation of two parameters derived from two independent experimental outputs, viz., lifetimes of the positrons and the lineshape of the annihilation gamma ray spectrum. The S and W parameters are derived according to

$$S = \frac{\sum_{i=0}^{8} N(i)}{\sum_{i=0}^{175} N(i)} \text{ and } W = \frac{\sum_{i=20}^{50} N(i)}{\sum_{i=0}^{175} N(i)} \quad (4)$$

where $N(i)$ stands for the counts in the ith channel after subtraction of the background and one channel corresponded to 80 eV ($i = 0$ is the 511 keV peak channel). The S versus W plot shown in Fig. 9 is however a straight line, indicating that the positron trapping sites are qualitatively of the same type throughout the Sc doping (upto 0.6 wt.%) and the changes taking place around 0.2 wt.% Sc concentration are related to either

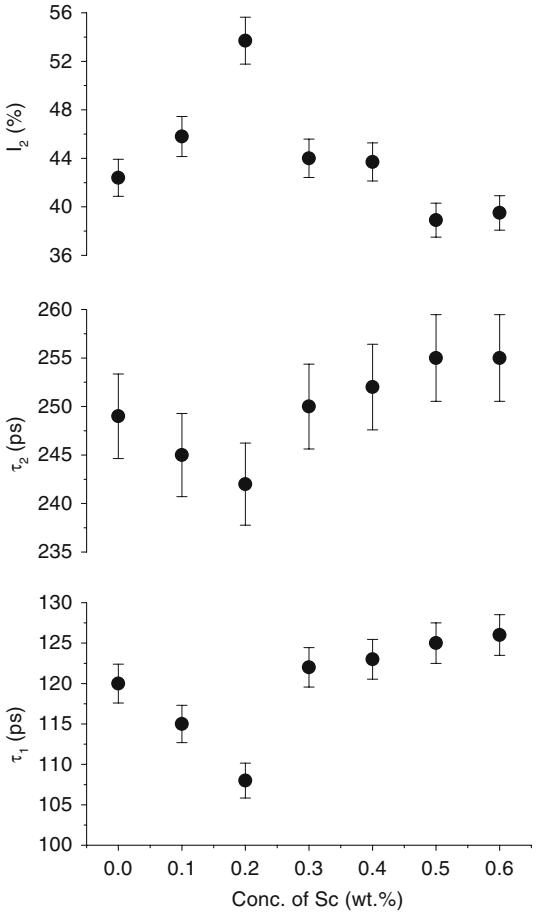

Fig. 7 The positron lifetimes τ_1 and τ_2 and the relative intensity I_2 versus the concentration of doped scandium

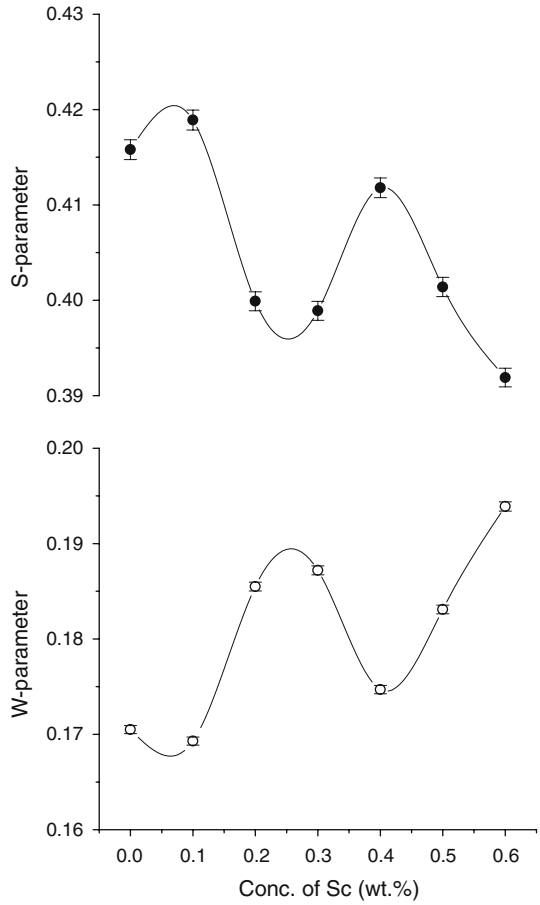

Fig. 8 The S and W parameters versus the concentration of doped scandium

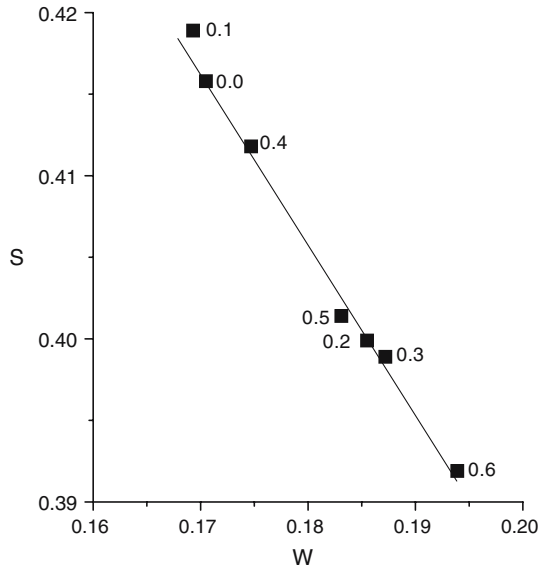

Fig. 9 The *S*–*W* plot versus the concentration of doped scandium

a change in the size of the defect or its concentration. This is also supported by the variation of I_2 (Fig. 7), which is increasing in the initial stages. The addition of Sc atoms results in replacing some Al atoms in the alloy and, in the process, there is the likelihood of formation of vacancy impurity complex type defects within the alloy system. The vacancy-solute atom complexes can also segregate over the heterogeneous environments like the hitherto mentioned grain boundaries and interfaces. The formation of complexes has enhanced the probability of trapping of positrons at these sites. The presence of an impurity atom, especially with larger number of electrons would then reduce the positron lifetime. This is especially true in the case of Sc when compared to Mg because of the presence of one extra *d* electron in the former in addition to the eight inner shell electrons. Unfortunately, positron lifetime data on Sc is scarce in literature and a work reported by Rodda and Stewart in 1963 suggests that it is 56 ± 3 ps larger than that of Al [27]. If we take the lifetime in Al as 165 ps [24], the value in the case of Sc is 221 ps. But this is just close to the positron lifetime in Mg, which has been reported as 225 ps [23]. Therefore it will be practically impossible to identify from positron lifetime measurements the presence of Sc atoms occupying the sites previously occupied by Mg or forming separate clusters of their own.

Since *S* and *W* parameters are more sensitive to the chemical nature of the surroundings of positron traps and since their variation with Sc concentration indeed reflects a change around 0.2, there ought to be a transition of chemical environment of the neighbouring scandium atoms. While scandium vacancy complexes can account for the decrease in positron lifetime, the increase in lifetimes beyond 0.2% is a certain indication of sources of traps like interfaces. Accounting for the presence of scandium inside such a matrix otherwise is not possible, considering the fact that the actual change in the positron lifetimes is not very high. The previous evidence of the formation of scandium vacancy complexes further adds to the validity of the above explanations [28]. From Fig. 7, it is seen that the maximum changes in τ_1 and τ_2 are only 18 ps and 13 ps, respectively.

With increasing Sc concentration, the positron lifetimes τ_1 and τ_2 have been found to increase and there is a conspicuous decrease in the relative intensity I_2. The formation of vacancy–scandium atom complexes and the decoration of the grain boundaries by the Sc atoms should have reached a level of saturation at 0.2% concentration, as otherwise the decreasing trend in the positron lifetimes should have continued. The CDBS curves obtained for $x = 0.2$ and 0.6 perfectly overlap, as shown in Fig. 10, indicating that the elemental environments around the positron traps are not affected but at the same time the trap size has increased slightly (as shown by an increase in the lifetime) while the trap concentration has decreased. This is significant in view of the fact that increasing Sc may lead to the formation of Al_3Sc in the alloy system. Interestingly, one would observe that both the CDBS

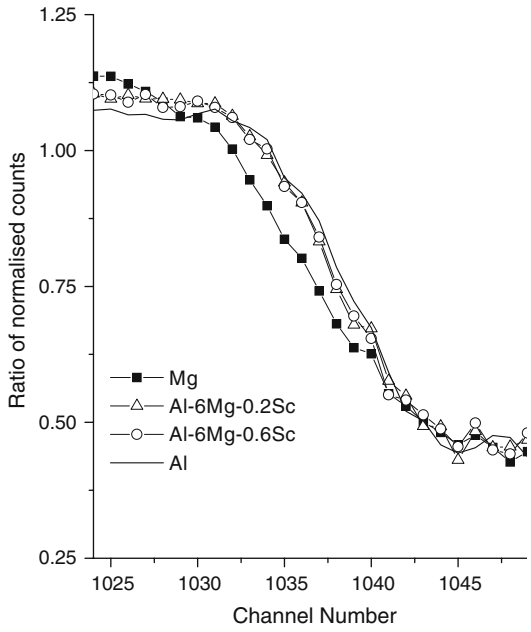

Fig. 10 CDB spectra of Al, Mg, Al–6Mg–0.2Sc and Al–6Mg–0.6Sc

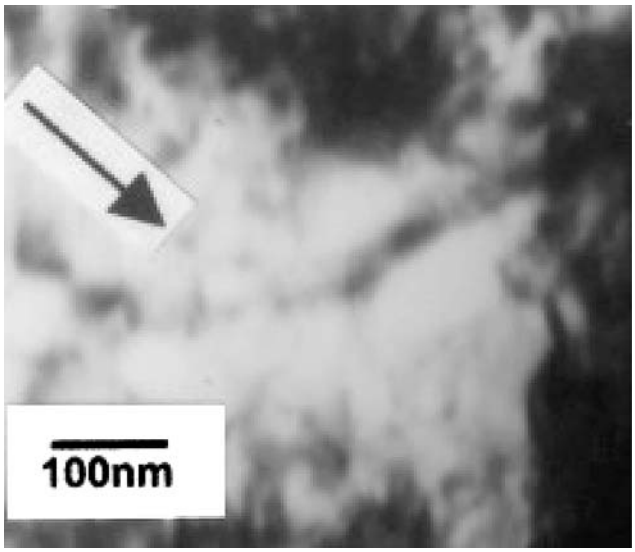

Fig. 11 Transmission electron micrograph of the cast Al–6Mg–0.6Sc alloy from a thin foil different from that of Fig. 4

curves for $x = 0.2$ and 0.6 lie very close to that for pure aluminium. It has the implication that the positron annihilation event due to scandium occurs in a chemical environment essentially rich in aluminium. This hints upon the formation of Al_3Sc precipitates in the alloy system when Sc concentration exceeds 0.2 wt%. This argument is well justified by the presence of fine Al_3Sc precipitates, as shown in the transmission electron micrographs of the as-prepared Al–6Mg–0.6Sc alloy (Figs. 4, 11). Thus it may be stated that upto 0.2% Sc, its increased core electrons reduce the positron lifetime. Beyond this, the formation of separate cluster/entity of Al_3Sc type creates additional interfaces to increase the positron lifetime. With increase in Sc concentration, the size of the clusters increases, the specific surface area decreases, and hence I_2 decreases. It appears that the decrease in positron lifetime due to the higher number of core electrons in Sc reached a saturation value at a threshold Sc concentration of 0.2% as otherwise the trend of decrease would have continued.

The S and W parameters have shown an additional positron-defect interaction stage after a Sc concentration of 0.4, which was not visible in the variation of the lifetimes or their intensities (Figs. 7, 8.). Interestingly, the S–W plot shown in Fig. 9 however did not show any deviation, ruling out the possibility of any difference in the nature of the positron trapping sites.

The results of isochronal annealing

Further insight into the interaction between the doped Sc atoms and the $Al_{94-x}Mg_6Sc_x$ (or Al–6Mg–xSc) are obtained after performing isochronal annealing on two of the samples selected on the basis of the maximum disparity between the measured positron annihilation parameters. They were the samples with Sc concentration of 0.2 and 0.6. For convenience, the Al–6Mg–0.2Sc sample is hereafter referred as Sc-2 and Al–6Mg–0.6Sc as Sc-6.

The shorter lifetime τ_1 increases with the annealing temperature in both the samples (Fig. 12.). However, τ_1 drastically increases upon annealing the Sc-2 sample even at 373 K and its value is close to that in the other sample, Sc-6; whereas the change in τ_1 during this temperature interval in the Sc-6 sample is only marginal. This means that the sample Sc-2 upon annealing at 373 K attains the same type of structural configuration as that of Sc-6 so far as positron annihilation is concerned. Thus temperature and added doping of Sc atoms impart the same effect to the original sample Al–6Mg–xSc. The sudden increase in τ_1 of Sc-2 sample at 373 K is a clear indication that more number of similar positron traps are created due to heating and this has overbalanced the decreasing effect of τ_1 due to the increased number of core electrons in Sc. Following the previous argument, it is conjectured that during the annealing, precipitation sets in to produce semi-coherent boundaries. These act as traps for positrons to lead to sudden increase in τ_1. Transmission electron microstructure of Sc-2 sample gives evidence of precipitate formation upon annealing, for example, at 473 K (Fig. 3). It has been already clarified that the decrease

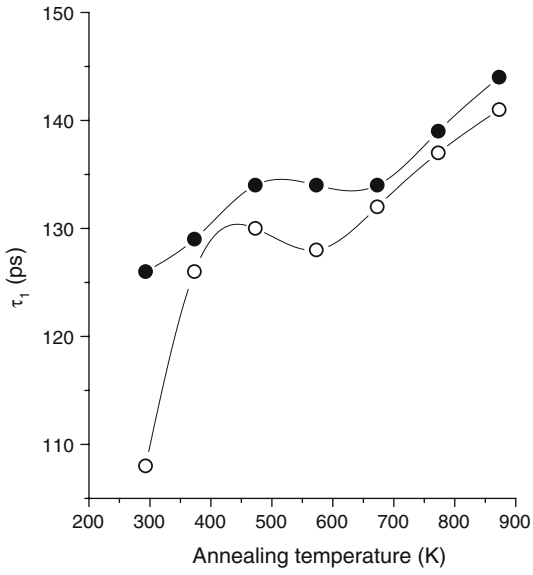

Fig. 12 The variation of the shorter lifetime τ_1 with isochronal annealing temperature for Al–6Mg–0.2Sc (*open circles*) and Al–6Mg–0.6Sc (*solid circles*)

of τ_1 (Fig. 7) during the initial increase (x) of the Sc concentration up to 0.2 wt.% results from the formation of Sc–vacancy complexes. Hence the increase of the same with annealing temperature (Fig. 12) is a clear indication of the dissociation of such complexes. The Sc atoms, which are thus dissociated from the binding vacancies, will now involve themselves in building new precipitate configuration, presumably of the Al_3Sc type. Figure 13 shows the increase in resistivity of Sc-2 alloy. Resistivity is responsive to atomic scale events and so the observed increase in resistivity can be supposed to be related to the hypothesis that scandium vacancy complex dissociates upon annealing and releases vacancies. The availability of vacancies entails the possibility of formation of Al_3Sc precipitates through reverse vacancy migration. The concurrent achievement of hardness maximum due to ageing the same alloy further corroborates the above idea (Fig. 14) [29]. As is evidenced in Fig. 11, the precipitates of Al_3Sc are already present in the as-prepared Sc-6 sample due to its high Sc concentration. The structural configurations in the two samples have now become identical and seem to remain stable during the annealing from 373 K to 673 K. Beyond this temperature, τ_1 rises further and then saturates. Considering such a significant increase, we cross-checked these values by reversing the Eqs. (1) and (2) to get the anticipated value of τ_f as

$$\tau_f = \frac{\tau_1\tau_2(I_1 + I_2)}{\tau_1 I_2 + \tau_2 I_1} \tag{5}$$

from the measured values of τ_1, τ_2, I_1 and I_2. This turned out to be 167 ps, which is close to the value 169 ps that had been earlier estimated for the bulk Al–6Mg. Incidentally, this value may also be arrived at if we consider trapping of positrons at the vacancies present in the precipitates of Sc (i.e., Al_3Sc). Thus positron lifetime measurements clearly reveal the formation and growth of Al_3Sc in scandium doped Al–6Mg alloy. It may be noted that the CDBS curve for the Sc-2 and Sc-6 samples, after the isochronal annealing till 873 K, are now moving closer to Mg, as shown in Fig. 15. This means more number of positrons are now annihilating at environments rich in Mg and this can happen only when the incoherent precipitates of Al–Mg intermetallics form more in number and grow in size. The presence of Mg_5Al_8 in the transmission electron microstructure of annealed Al–6Mg (Sc) alloy is supportive of nucleation and growth of

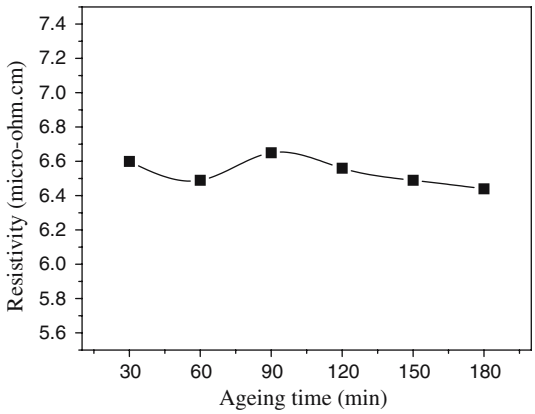

Fig. 13 Variation of the resistivity of the Sc-2 sample with aging time at 373 K

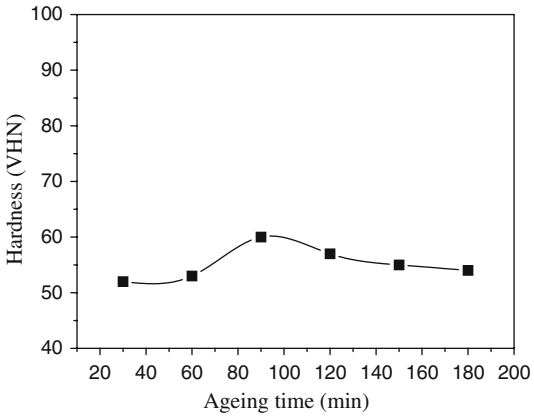

Fig. 14 Variation of hardness of the Sc-2 sample with aging time at 373 K

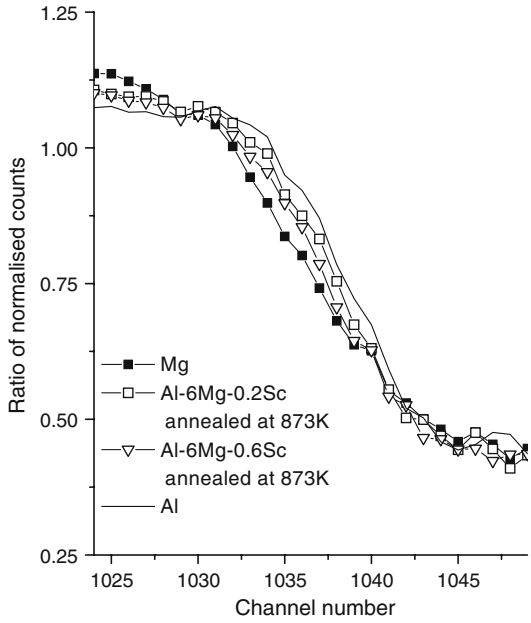

Fig. 15 CDB spectra of Al, Mg, Al–6Mg–0.2Sc and Al–6Mg–0.6Sc after the isochronal annealing at 873 K

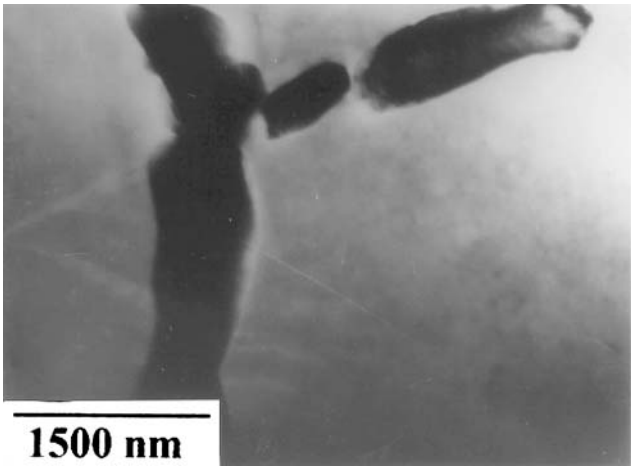

Fig. 16 Transmission electron microstructure of Sc-2 alloy annealed at 673 K showing Mg_5Al_8 particles

magnesium aluminide in the experimental alloy upon annealing at elevated temperature (Fig. 16). The release of vacancies by decomposition of Sc-vacancy complex aids in the transport of Mg atoms resulting in formation and growth Mg rich precipitates. In fact, with increasing annealing temperature, the enhanced mobility of Mg atoms has been responsible for fresh nucleation and growth of magnesium aluminides (Fig. 16).

The above arguments are further supported by the nature of variation of the longer component τ_2 and its intensity I_2 (Figs. 17, 18.). After the annealing at 373 K, τ_2 in Sc-2 attains an identical value as that in

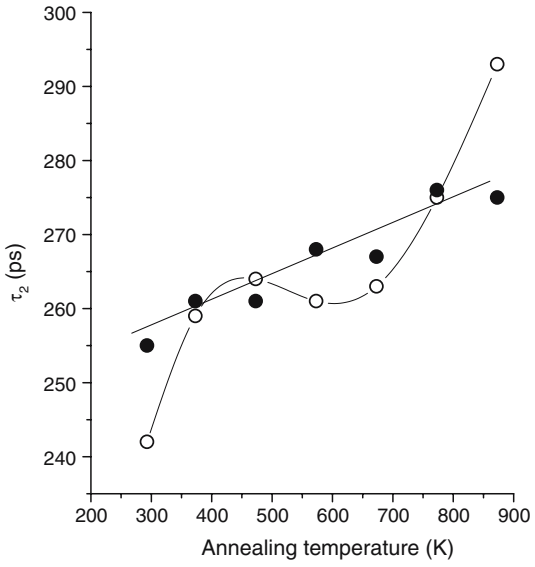

Fig. 17 The variation of the longer lifetime τ_2 with isochronal annealing temperature for Al–6Mg–0.2Sc (*open circles*) and Al–6Mg–0.6Sc (*solid circles*)

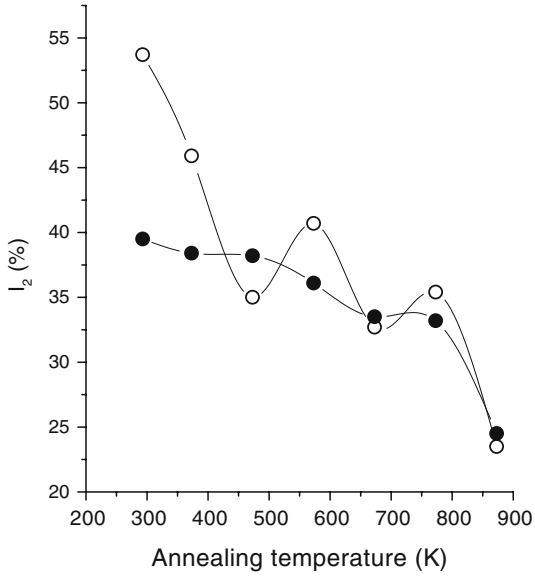

Fig. 18 The variation of the relative intensity I_2 with isochronal annealing temperature for Al–6Mg–0.2Sc (*open circles*) and Al–6Mg–0.6Sc (*solid circles*)

Sc-6. In the Sc-6 sample, further variation of τ_2 is a steady increase, showing the effect of coalescence of the precipitates. The sharp rise in τ_2 for the Sc-2 sample after 673 K is not clearly understood at this stage. However, a concomitant increase in the corresponding intensity I_2 within 673 K–773 K is an indication of the appearance of fresh precipitates of Al–Mg intermetallics and misfit dislocations at the new interfaces are now responsible for the increase of τ_2 and I_2. The plateau of τ_2 between 473 K and 573 K in Sc-2 alloy shows a positron lifetime above the bulk lifetime in Al. This is an indication of entrapment of positrons by lattice defects. Doped scandium atoms bind with vacancies and apart from being contained within the bulk alloy matrix the solute atom vacancy complexes are also present at the inter-phase boundaries within $\alpha + \beta$ eutectic. The amount of scandium vacancy complexes obviously depends upon the number of available quenched-in vacancies. When scandium is present in excess, the scandium atoms are neighboured by stoichiometrically adequate number of aluminium atoms to form Al_3Sc type of precipitates. On heating, the scandium vacancy complex dissociates and nucleation of Al_3Sc takes place. The released vacancies are subsequently available for transport of solute atoms at elevated temperatures.

It is now possible to consider the annealed alloy to be composed of a solid solution matrix embedded with the newly formed precipitates of Sc and Mg. Both types of precipitates are identically responsive to interaction with positrons. The intensity I_2 falls steadily

in both the cases due to the reduction in the net grain interfacial area as a consequence of expected coarsening of smaller particles into larger ones while heating to higher temperatures.

While the continued coarsening has led to a decrease in I_2, heating above 673 K has definitely increased the vibrational energy of the constituent atoms and deeper positron traps viz., thermal vacancies are considered responsible for the corresponding increase in τ_2. The dissolution of any precipitate is not probably the cause, as it would have led to a sharp change in slope of variation in positron lifetime in Sc-6 alloy (Fig. 17). Its straight-line nature corroborates that the increase of temperature has led to the formation of more thermal vacancies.

The *S*-parameter variation versus annealing temperature shown in Fig. 19 indicates identical recovery stages for both the samples at higher temperatures. While the disparity in the initial stages is attributed to the interaction between scandium and vacancies in Sc-2 alloy, the abnormal depression in *S* (and a corresponding peak of the *W*-parameter versus annealing temperature graph shown in the same Fig. 19) is assigned to the annihilation of positrons at precipitate–matrix interfaces. It should be however added that the *S*–*W* plot, shown in Fig. 20, is again a straight line indicating that the predominant annihilation sites are the grain interfaces of the incoherent Mg precipitates.

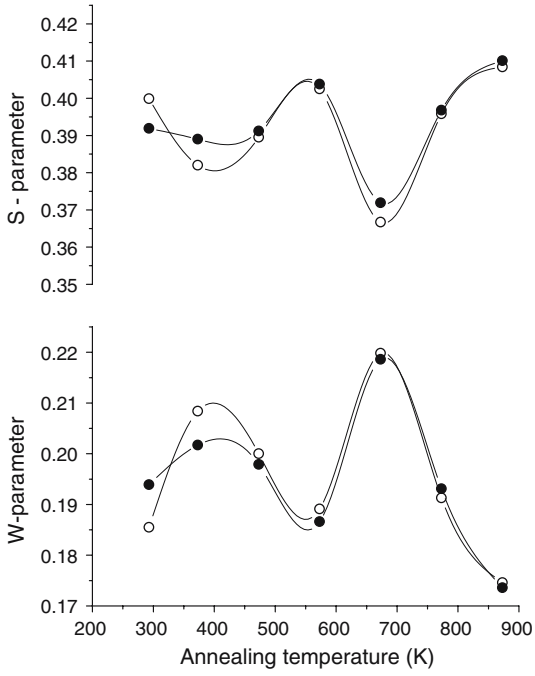

Fig. 19 The variation of the *S* and *W* parameters with isochronal annealing temperature for Al–6Mg–0.2Sc (*open circles*) and Al–6Mg–0.6Sc (*solid circles*)

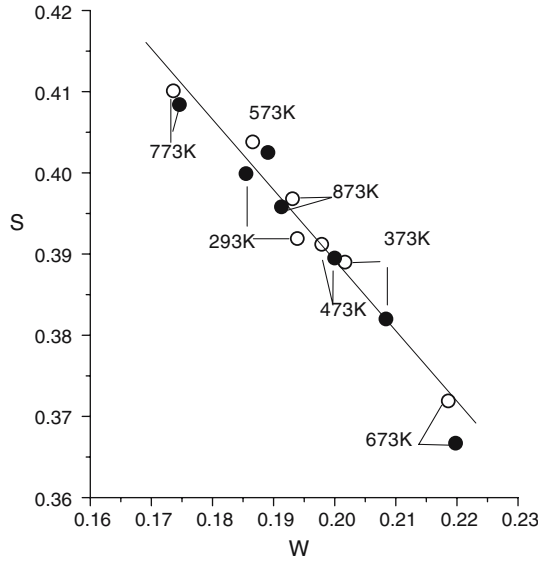

Fig. 20 The *S*–*W* plot versus the isochronal annealing temperature of the two samples Al–6Mg–0.2Sc (*open circles*) and Al–6Mg–0.6Sc (*solid circles*)

Conclusions

The positron lifetime spectroscopic results, together with the CDBS data, on the effects of doping Sc atoms inside the Al–6Mg matrix presented in this paper reveal that the interfaces between primary α-dendrite and the interspersed $\alpha + \beta$ eutectic act as the dominant positron trapping site in the undoped matrix. Addition of Sc replaced some of the Al atoms, leading to the formation of Sc-vacancy complexes. Strangely, this complex formation is not encouraged by the system beyond a Sc concentration of 0.2 wt.% and the surplus Sc atoms arrange themselves to form atomic arrays presumably neighboured by Al atoms. From the study on isochronal annealing of two samples of Sc concentration 0.2 and 0.6 wt.%, it was found that the Sc-vacancy complexes dissociate at higher temperature. The Sc atoms finally form their own precipitate Al_3Sc. These alongwith the undissolved incoherent Mg precipitates, if any, act as the predominant positron trapping sites. The precipitates of magnesium aluminide freshly form and grow at elevated temperatures and this is aided by the preceding formation of Sc precipitates, which is accompanied with the release of vacancies.

References

1. Aiura T, Sugawara N, Miura Y (2000) Mater Sci Eng A 280:139
2. Gaber A, Afify N (1992) J Mater Sci 27:1342

3. Toropova LS, Eskin DG, Kharakterova MI, Dobatkina TV (1998) Advanced aluminium alloys containing scandium. Gordon and Breach Science Publishers, Amsterdam, p 39
4. Aluminium–magnesium (5000) alloys, knowledge article, www.Key-To-Metals.com, p 1
5. Lorimer GW, Nicholson RB (1969) The mechanism of phase transformation in crystalline solids. Monograph and Robert Series No. 33. The Institute of Metals, p 36
6. Ohta M, Yamada M, Kanadani T, Sakakibara A (1987) Mater Trans Jim 28:615
7. Gaber AF, Afify N, Gadalla A, Mossad A (1999) High Temp–High Press 31:613
8. Mcnelley TR, Lee EW, Mills ME (1986) Met Trans A 17:1035
9. Lee EW, Mcnelley TR, Stengel AF (1986) Met Trans A 17:1043
10. Polmear IJ (1987) Mater Sci Forum 13/14:195
11. Sawtell RR, Jensen CL (1990) Met Trans A 21:421
12. Drits ME, Pavlenko SV, Toropova LS, Bykov YuG, Ber LB (1981) Soviet Phys Dokl 26:344
13. Elagin VI, Zakharov VV, Rostova TD (1983) Metally Term Obbrab Met 7:57
14. Willy LA (1971) United States Patent No. 3,619,181
15. Dirts MD, Toropova LS, Bykov YuG (1983) Metally Term Obbrab Met 7:60
16. Kaygorodova LI, Domashnikov VP (1989) Fiz Metal Metalloved 68:792
17. Dupasquier A, Somoza A (1995) Mater Sci Forum 175–178:35 and references therein
18. Mukherjee P, Nambissan PMG, Sen P, Barat P, Bandyopadhyay SK (1999) J Nucl Mater 273:238
19. Dlubek G (1987) Mater Sci Forum 13–14:11
20. Banerjee MK, Datta S (2000) J Mater Charac 44:277
21. Kirkegaard P, Eldrup M, Mogensen OE, Pedersen NJ (1981) Comput Phys Commun 23:307
22. Sachdeva A, Sudarshan K, Pujari PK, Goswami A, Sreejith K, George VC, Pillai CGS, Dua AK (2004) Diam Relat Mater 13:1719
23. Mackenzie IK (1983) In: Brandt W, Dupasquier A (eds) Positron solid state physics. North Holland, Amsterdam, p 196
24. Puska MJ, Nieminen RM (1983) J Phys F Met Phys 13:333
25. Hautojarvi P, Corbel C (1995) In: Dupasquier A, Mills AP Jr (eds) Positron spectroscopy of solids. Ios Press, Amsterdam, p 491
26. Bergersen B, Pajanne E, Kubica K, Stott MJ, Hodges CH (1974) Solid St Commun 15:1337
27. Rodda JL, Stewart MG (1963) Philos Mag 131:255
28. Kaygorodova LI, Domashnikov VP, Shashkov OD (1989) Fiz Metal Metalloved 67:786
29. Kaiser MS, Banerjee MK (2006) Indian Foundry J 52:29